

SELF-COMPOSING NEURAL OPERATORS WITH DEPTH AND ACCURACY SCALING VIA ADAPTIVE TRAIN-AND-UNROLL APPROACH*

JUNCAI HE [†], XINLIANG LIU [‡], AND JINCHAO XU [§]

Abstract. In this work, we propose a novel framework to enhance the efficiency and accuracy of neural operators through self-composition, offering both theoretical guarantees and practical benefits. Inspired by iterative methods in solving numerical partial differential equations (PDEs), we design a specific neural operator by repeatedly applying a single neural operator block, we progressively deepen the model without explicitly adding new blocks, improving the model’s capacity. To train these models efficiently, we introduce an adaptive train-and-unroll approach, where the depth of the neural operator is gradually increased during training. This approach reveals an accuracy scaling law with model depth and offers significant computational savings through our adaptive training strategy. Our architecture achieves state-of-the-art (SOTA) performance on standard benchmarks. We further demonstrate its efficacy on a challenging high-frequency ultrasound computed tomography (USCT) problem, where a multigrid-inspired backbone enables superior performance in resolving complex wave phenomena. The proposed framework provides a computationally tractable, accurate, and scalable solution for large-scale data-driven scientific machine learning applications.

Key words. Operator learning, self-composition, multigrid, efficient training, ultrasound computed tomography

MSC codes. 68Txx, 65Mxx

1. Introduction. Partial differential equation (PDE) models are ubiquitous in physics, engineering, and other disciplines. Many scientific and engineering fields rely on solving PDEs, such as optimizing airfoil shapes for better airflow, predicting weather patterns by simulating the atmosphere, and testing the strength of structures in civil engineering. Tremendous efforts have been made to solve various PDEs arising from different areas. Solving PDEs usually requires designing numerical methods that are tailored to the specific problem and depend on the insights of the model. However, deep learning models have shown great promise in solving PDEs in a more general and efficient way. Recently, several novel methods have been developed to directly learn the operator (mapping) between infinite-dimensional parameter and solution spaces of PDEs. Notable examples include DeepONet [35], which employs a branch-trunk architecture grounded in universal approximation theory [5], and the Fourier Neural Operator (FNO) [33], which parameterizes global convolutional operators using a fast Fourier transform. This line of research has expanded rapidly, yielding variants like geo-FNO [32] for complex geometries, the Latent Spectral Model (LSM) [46] that operates in a learned latent space, and Multiwavelet-based Transformers (MWT) [16] using wavelet transforms. Concurrently, attention mechanisms, popularized by Transformers [45], were adapted for operator learning, as seen in Galerkin-type attention models [3] and the General Neural Operator Transformer (GNOT) [20], which introduces heterogeneous normalized attention for handling multiple input functions and irregular meshes. More recently, explicitly convolution-based architectures have also

*Submitted to the editors DATE.

Funding: This work was funded by the KAUST research baseline.

[†]Yau Mathematical Sciences Center, Tsinghua University, Haidian District, Beijing 100084, China. (jche@tsinghua.edu.cn).

[‡]Ocean University of China, Qingdao, Shandong 266100, China. (xinliang.liu@ouc.edu.cn).

[§]King Abdullah University of Science and Technology, Thuwal, Saudi Arabia. (jinchao.xu@kaust.edu.sa)

been proposed as neural operators [42], and scalable approaches like Transolver++ [37] have demonstrated the ability to handle million-scale geometries for industrial applications. Additionally, specialized frameworks for complex geometries include Point Cloud Neural Operators (PCNO) [50], which efficiently handle variable domains with topological variations. MIONet is incorporated into classical iterative solvers, enhancing their efficiency [28, 26]. The NINO [19] has demonstrated how neural operators can learn to integrate traditional numerical techniques with Newton nonlinear solvers, effectively learning the nonlinear mapping at each iteration for multiple solutions.

These approaches can be broadly categorized. Spectral-type neural operators (e.g., FNO, MWT, LSM) leverage global operations and have shown promising results, supported by universal approximation theorems [29, 31]. However, they often struggle with complex boundary conditions, typically requiring boundary information to be encoded into the input data, and can exhibit a bias towards learning low-frequency components, as high-frequency modes might be truncated. In contrast, local and geometrical neural networks (e.g., ResNet [24, 25], UNet [43]) offer greater flexibility in managing diverse boundary conditions. Yet, these were not originally designed for operator learning of PDEs and often require a substantial number of parameters to achieve high accuracy. They can also act as high-pass filters, focusing on local features, which may limit their ability to capture long-distance dependencies crucial in many physical phenomena, unless specific mechanisms like large kernels are incorporated, which can be hard to train [10]. To bridge this gap, Liu *et al.* proposed the Hierarchical Attention Neural Operator (HANO), which mitigates spectral bias by adaptively coupling information across scales via attention, thereby boosting accuracy on challenging multiscale benchmarks [34]. Thus, although deep neural operators have shown great potential to learn complex patterns and relationships from data, and have been applied to fields like biomechanical engineering and weather forecasting [49, 40], they still face challenges regarding accuracy, flexibility with complex domains and boundary conditions, and parameter efficiency when compared to highly optimized classical numerical methods.

Motivated by the iterative nature of many classical PDE solvers, where a conventional procedure is repeated to progressively refine a solution, we pose the following question:

Question 1.1. Can we design and efficiently train an appropriate neural operator such that it repeats only a simple skeleton structure (low-cost) but can achieve high accuracy through this repetition?

This question draws inspiration from some of the most powerful techniques in scientific computing. Among all iterative methods for numerical PDEs, multigrid methods [18, 47, 44] are renowned for their efficiency, especially for elliptic PDEs. The connection between multigrid and deep learning was first noted in the original ResNet paper [24], citing multigrid as a rationale for residual connections. Subsequently, MgNet [22, 23] established deeper links, demonstrating that a linear V-cycle multigrid for the Poisson equation could be represented as a CNN. While MgNet and its adaptations have been explored for numerical PDEs [8, 54] and forecasting [55], a general and effective framework for integrating multigrid principles directly into operator learning for a broader class of PDEs has remained an open area. In this work, we aim to fundamentally integrate multigrid methodologies with operator learning based on a very general framework.

To address these challenges, we investigate the intrinsic properties of operator learning tasks governed by PDEs and propose a concise and elegant neural operator

architecture based on the concept of self-composition, directly inspired by iterative numerical methods. We introduce the general self-composing formulation $\mathcal{O}(\mathbf{v}) = \mathcal{P} \circ (\mathcal{G} \circ)^n \circ \mathcal{L}(\mathbf{v})$ for neural operators. This framework allows building deep operators with significant parameter sharing by repeatedly applying a backbone operator $\mathcal{G}(\cdot)$.

The concept of repeatedly applying a computational block shares similarities with several existing paradigms. Classical iterative methods for PDEs, such as Jacobi or Gauss-Seidel, inherently involve repeating a fixed update rule. Recurrent Neural Networks (RNNs) [9] also apply the same transition function repeatedly over a sequence. Algorithm unrolling [14] explicitly maps iterations of an optimization algorithm onto layers of a deep network. Our self-composing framework is distinct in several ways. While motivated by iterative PDE solvers, it focuses on learning the solution operator itself. Unlike standard RNNs which process sequential data, our model typically takes static function data as input and is primarily concerned with the final output after n compositions. Crucially, the backbone operator \mathcal{G} is shared across all n compositions, promoting significant parameter efficiency compared to standard deep networks or fully unrolled algorithms where parameters might vary per “iteration” or layer. Furthermore, our Train-and-Unroll strategy provides a specific, adaptive training mechanism tailored to this shared-parameter, variable-depth structure.

Another perspective in deep learning involves viewing networks as discretized ordinary differential equations (ODEs) [11, 17, 36, 6], where network depth corresponds to time steps. Pushing this to infinite depth leads to implicit neural network models like Deep Equilibrium Models (DEQs) [1, 13, 12], recently extended to implicit neural operators [38]. In these models, the output is found by solving for an equilibrium point. While elegant, the accuracy cannot be readily improved by further self-composition in the explicit, iterative manner our framework allows.

In this work, we introduce a novel general self-composing formulation for neural operators, defined as $\mathcal{O}(\mathbf{v}) = \mathcal{P} \circ (\mathcal{G} \circ)^n \circ \mathcal{L}(\mathbf{v})$, directly inspired by iterative numerical methods commonly employed in PDE solvers. This formulation facilitates the construction of deep neural operators through extensive parameter sharing by repeatedly applying a single backbone operator $\mathcal{G}(\cdot)$. We provide robust theoretical justification for our self-composing structure, including qualitative universal approximation results (see Theorem 2.1) and quantitative error reduction guarantees as the composition depth n increases (see Theorem 2.3). Additionally, we introduce an efficient adaptive training technique, termed the Train-and-Unroll strategy, which progressively increases the composition depth n throughout training, effectively leveraging previously learned weights from shallower network structures. To empirically demonstrate the parameter efficiency and effectiveness of our proposed self-composing structure, we apply it to benchmark Darcy flow problems, where our model exhibits significant advantages. Moreover, we further specialize our framework by designing an MgNet-inspired backbone augmented with an Adaptive Convolution Mechanism tailored specifically for the challenging Helmholtz equation arising in ultrasound computed tomography (USCT). The resulting neural operator achieves state-of-the-art performance, surpassing various general neural operator baselines and underscoring the practical applicability and versatility of our approach.

The remainder of this paper is structured as follows. Section 2 details the architecture of the self-composing neural operators, providing both qualitative and quantitative theoretical justifications alongside numerical experiments. Section 3 introduces the Train-and-Unroll strategy, our dynamic depth training algorithm for these operators. In Section 4, we describe a specific MgNet-inspired backbone designed for the Helmholtz equation. Section 5 presents numerical results that demonstrate the

efficiency and robustness of the proposed method. Finally, concluding remarks and future directions are discussed in Section 6.

2. Self-composing neural operators and theoretical analysis. In this section, we first introduce an abstract deep (fully connected) neural operator framework for mapping between (vector-valued) Hilbert function spaces, which can be generalized to Banach spaces. Then, we propose the self-composing neural operator architecture. Furthermore, we prove the universal approximation theory for this novel neural operator with some further theoretical and practical remarks and properties.

2.1. Abstract deep neural operators. We first denote $\mathcal{Z} = H^s(\Omega)$ be the Hilbert function on a bounded domain $\Omega \subset \mathbb{R}^d$ with the notation for the product space

$$\mathcal{Z}^n := \underbrace{\mathcal{Z} \otimes \mathcal{Z} \otimes \cdots \otimes \mathcal{Z}}_n.$$

Following the notation in [31, 21], we introduce the abstract deep neural operator framework $\mathcal{O} : \mathcal{Z}^{\tilde{d}} \mapsto \mathcal{Z}^{\tilde{d}}$ with a fully connected structure regarding neurons. To begin, we denote the bounded linear operator acting between these product spaces as $\mathcal{W} \in \mathcal{L}(\mathcal{Z}^n, \mathcal{Z}^m)$. To be more specific, the relation $[\mathcal{W}\mathbf{h}]_i = \sum_{j=1}^n \mathcal{W}_{ij} \mathbf{h}_j$ holds for $i = 1 : n, j = 1 : m$, where $\mathbf{h}_j \in \mathcal{Z}$ and $\mathcal{W}_{ij} \in \mathcal{L}(\mathcal{Z}, \mathcal{Z})$. Now, let us introduce $n_\ell \in \mathbb{N}^+$ for all $\ell = 1 : L$ as the number of neurons in ℓ -th hidden layer with $n_0 = \tilde{d}$ and $n_{L+1} = \tilde{d}$. Then, the deep neural operator $\mathcal{O}(\mathbf{v})$ with L hidden layers and n_ℓ neurons in ℓ -th layer is defined as

$$(2.1) \quad \begin{cases} \mathbf{h}^0(\mathbf{v}) = \mathbf{v} \in \mathcal{Z}^{n_0} \\ \mathbf{h}^\ell(\mathbf{v}) = \sigma(\mathcal{W}^\ell \mathbf{h}^{\ell-1}(\mathbf{v}) + \mathcal{B}^\ell) \in \mathcal{Z}^{n_\ell} \quad \ell = 1 : L \\ \mathcal{O}(\mathbf{v}) = \mathcal{W}^{L+1} \mathbf{h}^L(\mathbf{v}) + \mathcal{B}^{L+1} \in \mathcal{Z}^{n_{L+1}} \end{cases}$$

where $\mathcal{W}^\ell \in \mathcal{L}(\mathcal{Z}^{n_{\ell-1}}, \mathcal{Z}^{n_\ell})$ with $\mathcal{B}^\ell \in \mathcal{Z}^{n_\ell}$ and $\sigma : \mathbb{R} \mapsto \mathbb{R}$ defines the nonlinear point-wise activation. Unless otherwise specified, for simplicity, in the rest of the article, we call N as the width of the neural operator is $n_\ell = N$ for all $\ell = 1 : L$.

As shown in [21], although the above fully connected architecture is quite straightforward, it provides a very general framework for most existing neural operators. Basically, they mainly focus on how to parameterize the bounded linear operator $[\mathcal{W}^\ell]_{ij}$, for instance DeepONet [35], Fourier NO [33], Low-rank NO [30], Wavelet NO [16], Laplacian NO [4], Nonlocal NO [31], MgNO [21], etc.. In our work, we also propose a new parameterization mechanism with a natural motivation which will be introduced in the next section. Different from others, we also propose a new key architecture for building efficient and accurate deep neural operators motivated by iterative methods in solving numerical PDEs.

2.2. Self-composing neural operators motivated by iterative methods in solving PDEs. Typically, a standard PDE problem can be formulated as follows: Given a coefficient or parameter function $\mathbf{v} \in \mathcal{X}^{d_{\text{in}}}$, find the solution $\mathbf{u} \in \mathcal{Y}^{d_{\text{out}}}$ such that

$$(2.2) \quad \mathcal{D}(\mathbf{u}; \mathbf{v}) = 0,$$

where \mathcal{D} denotes the specific PDE operator involving derivatives and boundary information. Here, \mathcal{X} and \mathcal{Y} are Sobolev spaces defined on a bounded domain $\Omega \subset \mathbb{R}^d$, and d_{in} and d_{out} account for the diversity of different types of PDE problems. The

operator learning task, therefore, is to approximate the operator $\mathcal{O}^* : \mathcal{X}^{d_{\text{in}}} \rightarrow \mathcal{Y}^{d_{\text{out}}}$. In solving PDEs (both theoretically or numerically), we typically apply some iterative methods with certain initialization to approximate the solution as

$$(2.3) \quad \mathbf{u}^n = \mathcal{I}(\mathbf{u}^{n-1}; \mathbf{v}).$$

To express this iterative process as a self-composition, we define an augmented operator $\tilde{\mathcal{I}} : \mathcal{Y}^{d_{\text{out}}} \times \mathcal{X}^{d_{\text{in}}} \mapsto \mathcal{Y}^{d_{\text{out}}} \times \mathcal{X}^{d_{\text{in}}}$ whose action on the augmented state $(\mathbf{u}^{n-1}, \mathbf{v})$ is given by

$$(2.4) \quad \tilde{\mathcal{I}} \begin{pmatrix} \mathbf{u}^{n-1} \\ \mathbf{v} \end{pmatrix} := \begin{pmatrix} \mathcal{I}(\mathbf{u}^{n-1}; \mathbf{v}) \\ \mathbf{v} \end{pmatrix} = \begin{pmatrix} \mathbf{u}^n \\ \mathbf{v} \end{pmatrix}.$$

By applying this operator n times to the initial state $(\mathbf{u}^0, \mathbf{v})$, we obtain the state at the n -th iteration:

$$(2.5) \quad \begin{pmatrix} \mathbf{u}^n \\ \mathbf{v} \end{pmatrix} = (\tilde{\mathcal{I}} \circ)^n \begin{pmatrix} \mathbf{u}^0 \\ \mathbf{v} \end{pmatrix},$$

where $(\tilde{\mathcal{I}} \circ)^n$ denotes the self-composition of $\tilde{\mathcal{I}}$ for n times. If the iterative method \mathcal{I} is strictly monotonically convergent, we have $e_n < e_m$ for any $m < n$ where

$$(2.6) \quad e_n := \left\| \begin{pmatrix} \mathbf{u} \\ \mathbf{v} \end{pmatrix} - (\tilde{\mathcal{I}} \circ)^n \begin{pmatrix} \mathbf{u}^0 \\ \mathbf{v} \end{pmatrix} \right\|_{\mathcal{Y}^{d_{\text{out}}} \times \mathcal{X}^{d_{\text{in}}}} = \|\mathbf{u} - \mathbf{u}^n\|_{\mathcal{Y}^{d_{\text{out}}}}$$

Furthermore, for any linearly convergent iterative method \mathcal{I} , there exists $0 < \delta < 1$ such that $e_n \leq \delta^n e_0$. Motivated by this simple structure of self-composition and dynamic error decaying property, we propose the following fully connected deep neural operators with self-composing structure

$$(2.7) \quad \mathcal{O}(\mathbf{v}) = \mathcal{P} \circ (\mathcal{G} \circ)^n \circ \mathcal{L}(\mathbf{v})$$

where $\mathcal{L} : \mathcal{X}^{d_{\text{in}}} \rightarrow \mathcal{Z}^{\tilde{N}}$ and $\mathcal{P} : \mathcal{Z}^{\tilde{N}} \rightarrow \mathcal{Y}^{d_{\text{out}}}$ are two bounded linear operators for some $\tilde{N} \in \mathbb{N}^+$ and $\mathcal{G} : \mathcal{Z}^{\tilde{N}} \rightarrow \mathcal{Z}^{\tilde{N}}$ defines a vanilla deep fully connected neural operator with a fixed depth $L \in \mathbb{N}^+$, width $N \in \mathbb{N}^+$ and activation $\sigma(\cdot)$ as in equation 2.1 (with $n_0 = n_{L+1} = \tilde{N}$ because of the existing \mathcal{P} and \mathcal{L}). The components of this architecture parallel the augmented iterative method: the lifting operator \mathcal{L} creates an initial latent state from the input \mathbf{v} , analogous to creating the initial augmented state $(\mathbf{u}^0, \mathbf{v})$. The backbone operator \mathcal{G} acts as the neural analogue of the iterative update operator $\tilde{\mathcal{I}}$, and its repeated self-composition for n times mimics the iterative process. Finally, the projection operator \mathcal{P} extracts the final solution from the latent space, similar to retrieving \mathbf{u}^n from the final augmented state.

If $n = 1$, the neural operator defined in equation 2.7 degenerates to the standard deep fully connected neural operator as in equation 2.1. When $n \geq 2$, this self-composing neural operator architecture is quite different from the standard one. If the depth of \mathcal{G} is L , then one can also interpret $\mathcal{P} \circ (\mathcal{G} \circ)^n \circ \mathcal{L}$ as a fully connected neural operator with $n \times L$ hidden layers but sharing parameters along all n blocks where each block consists of a deep neural operator with L hidden layers. That is, the self-composing neural operator can efficiently save the memory cost for building a very deep neural operator. Given this special structure and efficiency in memory, we surprisingly still have the following universal approximation theory for self-composing neural operators.

2.3. Theoretical justification for self-composing neural operators. For simplicity, let us assume $d_{\text{in}} = d_{\text{out}} = 1$ and $\mathcal{O}^* : \mathcal{C} \subset \mathcal{X} \rightarrow \mathcal{Y}$ is a continuous operator on a compact domain \mathcal{C} . We first present the following universal approximation result for self-comprising neural operators with any fixed n .

THEOREM 2.1. *For any $n \in \mathbb{N}^+$ and $\epsilon > 0$, there exist $N, \tilde{N}, L \in \mathbb{N}^+$ with two bounded linear operators $\mathcal{L} : \mathcal{X} \rightarrow \mathcal{Z}^{\tilde{N}}$ and $\mathcal{P} : \mathcal{Z}^{\tilde{N}} \rightarrow \mathcal{Y}$ and a neural operator $\mathcal{G} : \mathcal{Z}^{\tilde{N}} \rightarrow \mathcal{Z}^{\tilde{N}}$ with ReLU activation function, L hidden layers and N neurons in each layer such that*

$$(2.8) \quad \sup_{\mathbf{v} \in \mathcal{C}} \|\mathcal{O}^*(\mathbf{v}) - \mathcal{P} \circ (\mathcal{G} \circ)^n \circ \mathcal{L}(\mathbf{v})\|_{\mathcal{X}} \leq \epsilon.$$

Here, \mathcal{Z} can be any function spaces that contain the constant function $\mathbf{1}(x)$ on Ω .

Before we prove the main theorem, we present the next important lemma about the approximation of a family of high-dimensional functions by the self-composition structure of deep ReLU neural networks.

LEMMA 2.2. *For any $\epsilon > 0$, $n \in \mathbb{N}^+$, and a sequence of constant numbers $\{c_i\}_{i=1}^m$ and functions $\{F_i(x)\}_{i=1}^m$ on $[0, 1]^k$, there exists a sequence of ReLU DNNs $\{\tilde{F}_i(x)\}$ such that*

$$\|F_i - \tilde{F}_i\|_{L^\infty([0,1]^k)} \leq \frac{\epsilon}{3mc_i}$$

for each $i = 1 : m$ with

$$\tilde{F}_i(x) = P_i \circ (g_i \circ)^n \circ L_i(x)$$

where $L_i : \mathbb{R}^k \mapsto \mathbb{R}^{\bar{k}}$ and $P_i : \mathbb{R}^{\bar{k}} \mapsto \mathbb{R}$ are affine mappings and $g_i : \mathbb{R}^{\bar{k}} \mapsto \mathbb{R}^{\bar{k}}$ is a deep ReLU neural network function with L hidden layers and \bar{k}_i neurons in each layer.

Proof. Given the approximation result in Theorem 1.3 in [52], for any $F_i(x)$ and $n_i \in \mathbb{N}^+$ with $i = 1 : m$, there exist ReLU DNNs $\hat{F}_i(x)$ such that

$$(2.9) \quad \|F_i - \hat{F}_i\|_{L^\infty([0,1]^k)} \leq 6\sqrt{k}\omega_{F_i} \left(n_i^{-1/k} \right) \leq \frac{\epsilon}{3mc_i},$$

with $\hat{F}_i(x) = P_i \circ (\hat{g}_i \circ)^{n_i} \circ L_i(x)$ where $P_i : \mathbb{R}^{\hat{k}} \mapsto \mathbb{R}$ and $L_i(x) : \mathbb{R}^k \mapsto \mathbb{R}^{\hat{k}}$ are linear maps with $\hat{k} = 3^k(5k+4) - 1$ and $\hat{g}_i : \mathbb{R}^{\hat{k}} \mapsto \mathbb{R}^{\hat{k}}$ are ReLU DNNs with $4^{k+5}k$ neurons and $3+2k$ hidden layers. Here, $\omega_f(r) := \sup_{\|x-y\| \leq r} |f(x) - f(y)|$ denotes the modulus of continuous function $f(x)$ on $[0, 1]^k$.

Thus, for all $\left\{ \frac{\epsilon}{3mc_i} \right\}_{i=1}^m$, one can take $\bar{n} = qn \geq \max_i \{n_i\}$ for some $q \in \mathbb{N}^+$. Consequently, calling Theorem 1.3 in [52] again, we have ReLU DNNs \bar{F}_i such that

$$(2.10) \quad \|F_i - \bar{F}_i\|_{L^\infty([0,1]^k)} \leq 6\sqrt{k}\omega_{F_i} \left(\bar{n}_i^{-1/k} \right) \leq 6\sqrt{k}\omega_{F_i} \left(n_i^{-1/k} \right) \leq \frac{\epsilon}{3mc_i}$$

for all $i = 1 : m$ with $\bar{F}_i(x) = \bar{P}_i \circ (\bar{g}_i \circ)^{n_i} \circ \bar{L}_i(x)$ where $\bar{P}_i : \mathbb{R}^{\bar{k}} \mapsto \mathbb{R}$ and $\bar{L}_i(x) : \mathbb{R}^k \mapsto \mathbb{R}^{\bar{k}}$ are linear maps with $\bar{k} = \hat{k} = 3^k(5k+4) - 1$ and $\bar{g}_i : \mathbb{R}^{\bar{k}} \mapsto \mathbb{R}^{\bar{k}}$ are ReLU DNNs with $4^{k+5}k$ neurons and $3+2k$ hidden layers.

Finally, we can finish the proof by taking $g_i = (\bar{g}_i \circ)^q$, $P_i = \bar{P}_i$, and $L_i = \bar{L}_i$ for all $i = 1 : m$. \square

With Lemma 2.2 on hand, we can present the proof for Theorem 2.1.

Proof. If $n = 1$, it degenerates to the classical approximation theorem of neural operators with only one hidden layer or a general deep neural operator architecture, which can be found in [31, 21].

Here, we are more interested in the case $n \geq 2$ since this requires a repeated composition of a fixed ReLU neural network. We split the proof to the following steps.

Finite-dimension approximation of \mathcal{O}^ by projection.* Since $\mathcal{C} \subset \mathcal{X}$ is a compact set and \mathcal{O}^* is continuous, we have the $\mathcal{O}^*(\mathcal{C})$ is also compact in \mathcal{Y} . Thus, for any $\epsilon > 0$, there are unit orthogonal basis function $\{\phi_1, \dots, \phi_m\} \subset \mathcal{Y}$ and continuous functionals $f_i : \mathcal{X} \mapsto \mathbb{R}$ for $i = 1 : m$ such that

$$(2.11) \quad \sup_{\mathbf{v} \in \mathcal{C}} \left\| \mathcal{O}^*(\mathbf{v}) - \sum_{i=1}^m f_i(\mathbf{v}) \phi_i \right\|_{\mathcal{Y}} \leq \frac{\epsilon}{3}.$$

Thus, we only need to prove that there is deep neural operator $\mathcal{O}_i = \mathcal{P}_i \circ (\mathcal{G}_i \circ)^n \circ \mathcal{L}_i$ such that

$$(2.12) \quad \sup_{\mathbf{v} \in \mathcal{C}} \|f_i(\mathbf{v}) \phi_i - \mathcal{O}_i(\mathbf{v})\|_{\mathcal{Y}} \leq \frac{2\epsilon}{3m}.$$

Parameterization (approximation) of \mathcal{X} with finite dimensions to discretize f_i . Since $\mathcal{X} = H^s(\Omega)$ and \mathcal{C} is compact, we can find $k \in \mathbb{N}^+$ such that

$$(2.13) \quad \sup_{\mathbf{v} \in \mathcal{C}} \left\| f_i(\mathbf{v}) \phi_i - f_i \left(\sum_{j=1}^k (\mathbf{v}, \varphi_j) \varphi_j \right) \phi_i \right\|_{\mathcal{Y}} \leq \frac{\epsilon}{3m} \quad \forall i = 1 : m,$$

where φ_i are the L^2 orthogonal basis in Sobolev space \mathcal{X} . Then, for a specific $f_i : \mathcal{X} \mapsto \mathbb{R}$, let us define the following finite-dimensional continuous function $F_i : \mathbb{R}^k \mapsto \mathbb{R}$ as

$$(2.14) \quad F_i(x) = f_i \left(\sum_{j=1}^k x_j \varphi_j \right), \quad \forall x \in [-M, M]^k,$$

where $M := \sup_i \sup_{\mathbf{v} \in \mathcal{C}} (\mathbf{v}, \varphi_i) < \infty$ because of the compactness of \mathcal{C} .

Universal approximation of F_i on $[-M, M]^k$ using Lemma 2.2. For any $n \geq 2$, by using the scaling and shifting transformation to map $[-1, 1]^k$ to $[0, 1]^k$ and calling Lemma 2.2 with $c_i = \|\phi_i\|_{\mathcal{Y}} = 1$, we have

$$(2.15) \quad \tilde{F}_i(x) = P_i \circ (g_i \circ)^n \circ L_i(x),$$

for any $i = 1 : m$, such that

$$(2.16) \quad \left\| F_i(x) - \tilde{F}_i(x) \right\|_{L^\infty([-M, M]^k)} \leq \frac{\epsilon}{3m}.$$

Construction of \mathcal{O}_i using the structure of \tilde{F}_i . Now, let us define \mathcal{O}_i as

$$(2.17) \quad \mathcal{O}_i(\mathbf{v}) = \mathcal{P}_i \circ (\mathcal{G}_i \circ)^n \circ \mathcal{L}_i(\mathbf{v}).$$

More precisely, we can take

$$(2.18) \quad \mathcal{L}_i(\mathbf{v}) = L_i \begin{pmatrix} (\mathbf{v}, \varphi_1) \mathbf{1}(x) \\ \vdots \\ (\mathbf{v}, \varphi_k) \mathbf{1}(x) \end{pmatrix}$$

where L_i comes from equation 2.15 when construct \tilde{F}_i and $\mathbf{1}(x) \in \mathcal{Z}$ denotes the constant function with value 1 everywhere on Ω . For $\mathcal{G}_i : \mathcal{Z}^{\tilde{k}} \mapsto \mathcal{Z}^{\tilde{k}}$, we denote the deep neural operator with ReLU activation function as

$$(2.19) \quad \mathcal{G}_i(\mathbf{v}) = \sigma(\mathcal{W}_i^L \sigma(\cdots \mathcal{W}_i^2 \sigma(\mathcal{W}_i^1 \mathbf{v} + \mathcal{B}_i^1) + \mathcal{B}_i^2) + \mathcal{B}_i^L).$$

Furthermore, noticing the definition of \mathcal{L}_i , we take \mathcal{W}_i^ℓ and \mathcal{B}_i^ℓ as

$$(2.20) \quad [\mathcal{W}_i^\ell]_{st} (a \mathbf{1}(x)) + [\mathcal{B}_i^\ell]_s = a [W_i^\ell]_{st} \mathbf{1}(x) + [b_i^\ell]_s \mathbf{1}(x),$$

where W_i^ℓ and b_i^ℓ are defined by g_i in equation 2.15 with

$$(2.21) \quad g_i(x) = \sigma(W_i^L \sigma(\cdots W_i^2 \sigma(W_i^1 x + b_i^1) + b_i^2) + b_i^L).$$

This leads to

$$(2.22) \quad \begin{aligned} (\mathcal{G}_i \circ)^n \circ \mathcal{L}_i(\mathbf{v}) &= \left((\mathcal{G}_i \circ)^n \circ L_i \begin{pmatrix} (\mathbf{v}, \varphi_1) \mathbf{1}(x) \\ \vdots \\ (\mathbf{v}, \varphi_k) \mathbf{1}(x) \end{pmatrix} \right) \\ &= \left((g_i \circ)^n \circ L_i \begin{pmatrix} (\mathbf{v}, \varphi_1) \\ \vdots \\ (\mathbf{v}, \varphi_k) \end{pmatrix} \right) \mathbf{1}(x) \\ &= \begin{pmatrix} c_{i,1}(\mathbf{v}) \mathbf{1}(x) \\ \vdots \\ c_{i,\tilde{k}}(\mathbf{v}) \mathbf{1}(x) \end{pmatrix} \end{aligned}$$

where $c_{i,p} : \mathcal{X} \mapsto \mathbb{R}$ are some continuous functionals.

Next, we can define

$$(2.23) \quad \mathcal{P}_i \begin{pmatrix} c_{i,1}(\mathbf{v}) \mathbf{1}(x) \\ \vdots \\ c_{i,\tilde{k}}(\mathbf{v}) \mathbf{1}(x) \end{pmatrix} = \left(P_i \begin{pmatrix} c_{i,1}(\mathbf{v}) \mathbf{1}(x) \\ \vdots \\ c_{i,\tilde{k}}(\mathbf{v}) \mathbf{1}(x) \end{pmatrix} \right) \phi_i.$$

In the end, we have

$$(2.24) \quad \begin{aligned} \mathcal{O}_i(\mathbf{v}) &= \mathcal{P}_i \circ (\mathcal{G}_i \circ)^n \circ \mathcal{L}_i(\mathbf{v}) \\ &= \left(P_i \circ (g_i \circ)^n \circ L_i \begin{pmatrix} (\mathbf{v}, \varphi_1) \\ \vdots \\ (\mathbf{v}, \varphi_k) \end{pmatrix} \right) \phi_i \\ &= \tilde{F}_i((\mathbf{v}, \varphi_1), \cdots, (\mathbf{v}, \varphi_k)) \phi_i. \end{aligned}$$

Triangle inequalities to finalize the proof:. Given the previous construction, we have

$$\begin{aligned}
(2.25) \quad & \sup_{\mathbf{v} \in \mathcal{C}} \|f_i(\mathbf{v})\phi_i - \mathcal{O}_i(\mathbf{v})\|_{\mathcal{Y}} \\
& \leq \sup_{\mathbf{v} \in \mathcal{C}} \left\| f_i(\mathbf{v})\phi_i - f_i \left(\sum_{j=1}^k (\mathbf{v}, \varphi_j) \varphi_j \right) \phi_i \right\|_{\mathcal{Y}} \\
& + \sup_{\mathbf{v} \in \mathcal{C}} \left\| f_i \left(\sum_{j=1}^k (\mathbf{v}, \varphi_j) \varphi_j \right) \phi_i - \mathcal{O}_i(\mathbf{v}) \right\|_{\mathcal{Y}} \\
& \leq \frac{\epsilon}{3m} + \sup_{\mathbf{v} \in \mathcal{C}} \left| f_i \left(\sum_{j=1}^k (\mathbf{v}, \varphi_j) \varphi_j \right) - \tilde{F}_i(((\mathbf{v}, \varphi_1), \dots, (\mathbf{v}, \varphi_k))) \right| \|\phi_i\|_{\mathcal{Y}} \\
& = \frac{\epsilon}{3m} + \sup_{\mathbf{v} \in \mathcal{C}} \left| F_i(((\mathbf{v}, \varphi_1), \dots, (\mathbf{v}, \varphi_k))) - \tilde{F}_i(((\mathbf{v}, \varphi_1), \dots, (\mathbf{v}, \varphi_k))) \right| \\
& \leq \frac{\epsilon}{3m} + \frac{\epsilon}{3m} = \frac{2\epsilon}{3m}.
\end{aligned}$$

As a result, we have

$$\begin{aligned}
(2.26) \quad & \sup_{\mathbf{v} \in \mathcal{C}} \left\| \mathcal{O}^*(\mathbf{v}) - \sum_{i=1}^m \mathcal{O}_i(\mathbf{v}) \right\|_{\mathcal{Y}} \\
& \leq \sup_{\mathbf{v} \in \mathcal{C}} \left(\left\| \mathcal{O}^*(\mathbf{v}) - \sum_{i=1}^m f_i(\mathbf{v})\phi_i \right\|_{\mathcal{Y}} + \sum_{i=1}^m \|f_i(\mathbf{v})\phi_i - \mathcal{O}_i(\mathbf{v})\|_{\mathcal{Y}} \right) \\
& \leq \frac{\epsilon}{3} + m \frac{2\epsilon}{3m} = \epsilon,
\end{aligned}$$

where \mathcal{O}_i has the structure as in equation 2.24. Since \mathcal{O}_i has a uniform depth, we can then concatenate them to a global neural operator

$$(2.27) \quad \mathcal{O}(\mathbf{v}) = \begin{pmatrix} \mathcal{P}_1 \\ \vdots \\ \mathcal{P}_m \end{pmatrix} \circ \left(\begin{pmatrix} \mathcal{G}_1 \\ \vdots \\ \mathcal{G}_m \end{pmatrix} \circ \right)^n \circ \begin{pmatrix} \mathcal{L}_1 \\ \vdots \\ \mathcal{L}_m \end{pmatrix} (\mathbf{v}).$$

with the same depth but neurons as the summation for each sub-structure. \square

For $n = 1$, this theorem degenerates to the most commonly used universal approximation theorem of classical neural operators, for example, [30, 21]. For any $n \geq 2$, this result has not been mentioned or discussed in any previous literature. One of the most challenging parts in the above theorem is the self-composition, or one can imagine $(\mathcal{G} \circ)^n$ as a neural operator with nL hidden layers where in which there is a sharing of parameters along each block which is a neural operator with L hidden layers.

Motivated by the iterative methods in solving numerical PDEs, we have a natural question of whether we can have higher accuracy by just self-composing a fixed size (depth and width) backbone without adding any new parameters. Under a further assumption to the operator \mathcal{O}^* , we have the following theorem that with suitable and fixed width and depth of \mathcal{G} and under a certain accuracy level, a larger n can achieve a lower error level.

THEOREM 2.3. *If \mathcal{O}^* is Lipschitz continuous, for any $\epsilon > 0$, there exist fixed $N, \tilde{N}, L \in \mathbb{N}^+$, such that for any $n \in \mathbb{N}^+$ we can find bounded linear operators $\mathcal{L} : \mathcal{X} \rightarrow \mathcal{Z}^{\tilde{N}}$ and $\mathcal{P} : \mathcal{Z}^{\tilde{N}} \rightarrow \mathcal{Y}$ and a ReLU neural operator $\mathcal{G} : \mathcal{Z}^{\tilde{N}} \rightarrow \mathcal{Z}^{\tilde{N}}$ with L hidden layers and N neurons in each layer satisfying*

$$(2.28) \quad \sup_{\mathbf{v} \in \mathcal{C}} \|\mathcal{O}^*(\mathbf{v}) - \mathcal{P} \circ (\mathcal{G} \circ)^n \circ \mathcal{L}(\mathbf{v})\|_{\mathcal{X}} \leq \epsilon + \frac{C_\epsilon}{\log(n)},$$

where C_ϵ depends on ϵ but is independent of n . Here, \mathcal{Z} can be any function spaces that contain the constant function $\mathbf{1}(x)$ on Ω .

The proof mainly follows the steps in the proof of Theorem 2.1. The key here is to use the Lipschitz condition of the target operator to get an explicit approximation rate in the final bound.

Proof. We split the proof as follows.

Finite-dimension approximation of \mathcal{O}^ by projection with Lipschitz continuity.* As in the first step in the proof of Theorem 2.1, those continuous functionals $f_i : \mathcal{X} \mapsto \mathbb{R}$ with orthogonal basis $\{\phi_1, \dots, \phi_m\} \subset \mathcal{Y}$ for $i = 1 : m$ are actually defined as

$$f_i(\mathbf{v}) := (\phi_i, \mathcal{O}^*(\mathbf{v}))_{\mathcal{Y}},$$

which are also Lipschitz continuous and

$$(2.29) \quad \sup_{\mathbf{v} \in \mathcal{C}} \left\| \mathcal{O}^*(\mathbf{v}) - \sum_{i=1}^m f_i(\mathbf{v}) \phi_i \right\|_{\mathcal{Y}} \leq \frac{\epsilon}{2}.$$

Moreover, it is easy to verify that the Lipschitz constants of f_i are all bounded by the Lipschitz constant of \mathcal{O}^* , which we denote as $\|\mathcal{O}^*\|$. Thus, we only need to prove that there is deep neural operator $\mathcal{O}_i = \mathcal{P}_i \circ (\mathcal{G}_i \circ)^n \circ \mathcal{L}_i$ such that

$$(2.30) \quad \sup_{\mathbf{v} \in \mathcal{C}} \|f_i(\mathbf{v}) \phi_i - \mathcal{O}_i(\mathbf{v})\|_{\mathcal{Y}} \leq \frac{\epsilon}{2m} + \frac{C_\epsilon}{m \log(n)},$$

where C_ϵ depends only on ϵ and \mathcal{O}^* and does not depend on n .

Parameterization (approximation) of \mathcal{X} with finite dimensions to discretize f_i . Since $\mathcal{X} = H^s(\Omega)$ and \mathcal{C} is compact, we can find $k \in \mathbb{N}^+$ such that

$$(2.31) \quad \sup_{\mathbf{v} \in \mathcal{C}} \left\| f_i(\mathbf{v}) \phi_i - f_i \left(\sum_{j=1}^k (\mathbf{v}, \varphi_j) \varphi_j \right) \phi_i \right\|_{\mathcal{X}} \leq \frac{\epsilon}{2m} \quad \forall i = 1 : m,$$

where φ_i are the orthogonal basis in $H^s(\Omega)$. Then, for a specific $f_i : \mathcal{X} \mapsto \mathbb{R}$, let us define the following finite-dimensional continuous function $F_i : \mathbb{R}^k \mapsto \mathbb{R}$ as

$$(2.32) \quad F_i(x) = f_i \left(\sum_{j=1}^k x_j \varphi_j \right), \quad \forall x \in [-M, M]^k,$$

where $M := \sup_i \sup_{u \in \mathcal{C}} (\mathbf{u}, \varphi_i) < \infty$ because of the compactness of \mathcal{C} . Furthermore, for each $i = 1 : m$, we notice that $F_i(x)$ is also Lipschitz continuous with Lipschitz constant less than the Lipschitz constant of f_i which has a uniform bound $\|\mathcal{O}^*\|$.

Quantitative approximation of F_i using self-composing deep ReLU neural networks. For any n , by using the scaling and shifting transformation to map $[-M, M]^k$ to $[-1, 1]^k$ and calling Theorem 1.3 in [52], we have

$$(2.33) \quad \tilde{F}_i(x) = P_i \circ (g_i \circ)^n \circ L_i(x),$$

for any $i = 1 : m$, such that

$$(2.34) \quad \left\| F_i(x) - \tilde{F}_i(x) \right\|_{L^\infty([-M, M]^k)} \leq \frac{12\sqrt{k}\|\mathcal{O}^*\|_{\mathcal{Y}}}{n^{1/k}} \leq \frac{C_\epsilon}{m \log(n)}$$

for sufficient large n and $C_\epsilon = \mathcal{O}(\sqrt{k}m\|\mathcal{O}^*\|)$ does not depend on n . Here, $L_i : \mathbb{R}^k \mapsto \mathbb{R}^{\tilde{k}}$ and $P_i : \mathbb{R}^{\tilde{k}} \mapsto \mathbb{R}$ are affine mappings and $g_i : \mathbb{R}^{\tilde{k}} \mapsto \mathbb{R}^{\tilde{k}}$ is a deep ReLU neural network function with L hidden layers and \tilde{k}_i neurons in each layer.

The construction of \mathcal{O}_i based on the structure of \tilde{F}_i , as well as the verification of the final results, closely follows the approach used in the proof of Theorem 2.1. Nevertheless, we include the details here for completeness.

Construction of \mathcal{O}_i using the structure of \tilde{F}_i . Now, let us define \mathcal{O}_i as

$$(2.35) \quad \mathcal{O}_i(\mathbf{v}) = \mathcal{P}_i \circ (\mathcal{G}_i \circ)^n \circ \mathcal{L}_i(\mathbf{v}).$$

More precisely, we can take

$$(2.36) \quad \mathcal{L}_i(\mathbf{v}) = L_i \begin{pmatrix} (\mathbf{v}, \varphi_1) \mathbf{1}(x) \\ \vdots \\ (\mathbf{v}, \varphi_k) \mathbf{1}(x) \end{pmatrix}$$

where L_i comes from equation 2.33 when construct \tilde{F}_i and $\mathbf{1}(x) \in \mathcal{Z}$ denotes the constant function with value 1. For $\mathcal{G}_i : \mathcal{Z}^{\tilde{k}} \mapsto \mathcal{Z}^{\tilde{k}}$, we denote the deep neural operator with ReLU activation function as

$$(2.37) \quad \mathcal{G}_i(\mathbf{v}) = \sigma(\mathcal{W}_i^L \sigma(\cdots \mathcal{W}_i^2 \sigma(\mathcal{W}_i^1 \mathbf{v} + \mathcal{B}_i^1) + \mathcal{B}_i^2) + \mathcal{B}_i^L).$$

Furthermore, noticing the definition of \mathcal{L}_i , we take \mathcal{W}_i^ℓ and \mathcal{B}_i^ℓ as

$$(2.38) \quad [\mathcal{W}_i^\ell]_{st} (a \mathbf{1}(x)) + [\mathcal{B}_i^\ell]_s = a [W_i^\ell]_{st} \mathbf{1}(x) + [b_i^\ell]_s \mathbf{1}(x),$$

where W_i^ℓ and b_i^ℓ are defined by g_i in equation 2.33 with

$$(2.39) \quad g_i(x) = \sigma(W_i^L \sigma(\cdots W_i^2 \sigma(W_i^1 x + b_i^1) + b_i^2) + b_i^L).$$

This leads to

$$(2.40) \quad \begin{aligned} (\mathcal{G}_i \circ)^n \circ \mathcal{L}_i(\mathbf{v}) &= \left((\mathcal{G}_i \circ)^n \circ L_i \begin{pmatrix} (\mathbf{v}, \varphi_1) \mathbf{1}(x) \\ \vdots \\ (\mathbf{v}, \varphi_k) \mathbf{1}(x) \end{pmatrix} \right) \\ &= \left((g_i \circ)^n \circ L_i \begin{pmatrix} (\mathbf{v}, \varphi_1) \\ \vdots \\ (\mathbf{v}, \varphi_k) \end{pmatrix} \right) \mathbf{1}(x) \\ &= \begin{pmatrix} c_{i,1}(\mathbf{v}) \mathbf{1}(x) \\ \vdots \\ c_{i,\tilde{k}}(\mathbf{v}) \mathbf{1}(x) \end{pmatrix} \end{aligned}$$

where $c_{i,p} : \mathcal{X} \mapsto \mathbb{R}$ are some continuous functionals.

Next, we can define

$$(2.41) \quad \mathcal{P}_i \begin{pmatrix} c_{i,1}(\mathbf{v})\mathbf{1}(x) \\ \vdots \\ c_{i,\tilde{k}}(\mathbf{v})\mathbf{1}(x) \end{pmatrix} = \left(P_i \begin{pmatrix} c_{i,1}(\mathbf{1}(x)) \\ \vdots \\ c_{i,\tilde{k}}(\mathbf{1}(x)) \end{pmatrix} \right) \phi_i.$$

In the end, we have

$$(2.42) \quad \begin{aligned} \mathcal{O}_i(\mathbf{v}) &= \mathcal{P}_i \circ (\mathcal{G}_i \circ)^n \circ \mathcal{L}_i(\mathbf{v}) \\ &= \left(P_i \circ (g_i \circ)^n \circ L_i \begin{pmatrix} (\mathbf{v}, \varphi_1) \\ \vdots \\ (\mathbf{v}, \varphi_k) \end{pmatrix} \right) \phi_i \\ &= \tilde{F}_i(((\mathbf{v}, \varphi_1), \dots, (\mathbf{v}, \varphi_k))) \phi_i. \end{aligned}$$

Triangle inequalities to finalize the proof. Given the previous construction, we have

$$(2.43) \quad \begin{aligned} &\sup_{\mathbf{v} \in \mathcal{C}} \|f_i(\mathbf{v})\phi_i - \mathcal{O}_i(\mathbf{v})\|_{\mathcal{Y}} \\ &\leq \sup_{\mathbf{v} \in \mathcal{C}} \left\| f_i(\mathbf{v})\phi_i - f_i \left(\sum_{j=1}^k (\mathbf{v}, \varphi_j) \varphi_j \right) \phi_i \right\|_{\mathcal{Y}} \\ &\quad + \sup_{\mathbf{v} \in \mathcal{C}} \left\| f_i \left(\sum_{j=1}^k (\mathbf{v}, \varphi_j) \varphi_j \right) \phi_i - \mathcal{O}_i(\mathbf{v}) \right\|_{\mathcal{Y}} \\ &\leq \frac{\epsilon}{2m} + \sup_{\mathbf{v} \in \mathcal{C}} \left| f_i \left(\sum_{j=1}^k (\mathbf{v}, \varphi_j) \varphi_j \right) - \tilde{F}_i(((\mathbf{v}, \varphi_1), \dots, (\mathbf{v}, \varphi_k))) \right| \|\phi_i\|_{\mathcal{Y}} \\ &= \frac{\epsilon}{2m} + \sup_{\mathbf{v} \in \mathcal{C}} \left| F_i(((\mathbf{v}, \varphi_1), \dots, (\mathbf{v}, \varphi_k))) - \tilde{F}_i(((\mathbf{v}, \varphi_1), \dots, (\mathbf{v}, \varphi_k))) \right| \\ &\leq \frac{\epsilon}{2m} + \frac{C_\epsilon}{m \log(n)}. \end{aligned}$$

As a result, we have

$$(2.44) \quad \begin{aligned} &\sup_{\mathbf{v} \in \mathcal{C}} \left\| \mathcal{O}^*(\mathbf{v}) - \sum_{i=1}^m \mathcal{O}_i(\mathbf{v}) \right\|_{\mathcal{Y}} \\ &\leq \sup_{\mathbf{v} \in \mathcal{C}} \left(\left\| \mathcal{O}^*(\mathbf{v}) - \sum_{i=1}^m f_i(\mathbf{v})\phi_i \right\|_{\mathcal{Y}} + \sum_{i=1}^m \|f_i(\mathbf{v})\phi_i - \mathcal{O}_i(\mathbf{v})\|_{\mathcal{Y}} \right) \\ &\leq \frac{\epsilon}{3} + m \left(\frac{\epsilon}{2m} + \frac{C_\epsilon}{m \log(n)} \right) = \epsilon + \frac{C_\epsilon}{\log(n)}, \end{aligned}$$

where \mathcal{O}_i has the structure as in equation 2.42. Since \mathcal{O}_i has a uniform depth, we can then concatenate them to a global neural operator

$$(2.45) \quad \mathcal{O}(\mathbf{v}) = \begin{pmatrix} \mathcal{P}_1 \\ \vdots \\ \mathcal{P}_m \end{pmatrix} \circ \left(\begin{pmatrix} \mathcal{G}_1 \\ \vdots \\ \mathcal{G}_m \end{pmatrix} \circ \right)^n \circ \begin{pmatrix} \mathcal{L}_1 \\ \vdots \\ \mathcal{L}_m \end{pmatrix} (\mathbf{v}). \quad \square$$

with the same depth but neurons as the summation for each sub-structure.

Noticing that N , \tilde{N} , and L are independent of n , the above theorem indeed verifies our previous intuition that with a certain budget for the backbone neural operator and under a certain accuracy level, the deeper (larger n), the better (lower accuracy).

Discussion on the convergence rate:. Theorem 2.3 provides a quantitative guarantee that the approximation error decreases as the number of compositions n increases, specifically at a rate of $O(1/\log(n))$ beyond a base error ϵ . While this confirms the benefit of deeper composition, the $1/\log(n)$ rate is asymptotically slow compared to error bounds for standard deep neural networks, where error often decreases polynomially or exponentially with explicit increases in width or depth (number of unique layers/parameters). This theoretical rate might suggest that the primary practical advantages of the self-composing structure stem from significant parameter sharing (acting as regularization) and the effectiveness of the Train-and-Unroll strategy (providing good initialization and progressive learning), rather than purely from the asymptotic error reduction due to n . The observed empirical error decay (e.g., Figure 2(b)) often appears faster than $1/\log(n)$, suggesting this bound might not be tight or that the constants involved play a significant role in practical regimes. Further investigation is needed to bridge the gap between this theoretical rate and empirical observations, potentially requiring different proof techniques or assumptions.

Numerically, the depth and accuracy scaling in Figure 2(b) verifies this theoretical result, showing error reduction with increasing n . Furthermore, we point out that the empirical scaling often appears closer to linear or sub-linear in the log-error plot, which is faster than the $O(1/\log(n))$ rate suggested by the theorem. This discrepancy highlights an interesting theoretical question for future investigation.

TABLE 1

Performance comparison for Darcy benchmarks. Performance are measured with relative L^2 errors ($\times 10^{-2}$) and relative H^1 errors ($\times 10^{-2}$).

Model	Time (s/iter)	Params (M)	Darcy smooth L^2 H^1		Darcy rough L^2 H^1		Multiscale L^2 H^1	
<i>Baseline methods</i>								
DilResNet	14.9	1.04	4.104	5.815	7.347	12.44	1.417	3.528
UNet	9.1	17.27	2.169	4.885	3.519	5.795	1.425	5.012
U-NO	11.4	16.39	0.492	1.276	1.023	3.784	1.187	5.380
MWT [†]	21.7	9.80	—	—	1.138	4.107	1.021	7.245
GT	38.2	2.22	0.945	3.365	1.790	6.269	1.052	8.207
LSM	18.2	4.81	0.601	2.610	2.658	4.446	1.050	4.226
<i>Neural operators w/o self-composition</i>								
FNO2D	7.4	2.37	0.684	2.583	1.613	7.516	1.800	9.619
FNO2D-self	7.4	0.56	0.751	3.102	1.981	8.115	2.064	11.070
MgNO	6.6	0.57	0.153	0.711	0.339	1.380	0.715	1.756
MgNO-self	6.7	0.17	0.187	0.813	0.371	1.514	0.800	2.871

[†] MWT only supports resolution with powers of two.

Note: FNO2D, U-NO and MWT’s performance are improved from originally reported due to usage of H^1 loss and scheduler. Runtime and parameter counts use Darcy rough as example case.

2.4. Experiments for self-composing neural operators. Table 1 offers initial experimental evidence for the practical benefits of the self-composing neural operator architecture (Equation 2.7). The results on Darcy flow benchmarks [33] and

multiscale benchmark [34] demonstrate that models employing shared-parameter self-composition (denoted with “-self”, e.g., FNO2D-self, MgNO-self) attain competitive approximation accuracy in both relative L^2 and H^1 errors when compared to their counterparts without parameter sharing (e.g., FNO2D [33], MgNO [21]) and other established baseline methods (e.g., UNet [43], U-NO [41], MWT [16]).

A key finding highlighted by Table 1 is the significant parameter efficiency of self-composed models. For instance, MgNO-self achieves its performance with approximately 0.17M parameters versus 0.57M for MgNO, while FNO2D-self uses approximately 0.56M parameters compared to 2.37M for FNO2D. This substantial reduction in model size, without a disproportionate loss in accuracy, underscores the parameter efficiency inherent in the self-composing design where a single backbone operator \mathcal{G}_θ is iteratively applied. This aligns with the motivation of developing deep and expressive, yet memory-efficient, neural operators, as discussed earlier in this section.

Further comprehensive numerical evaluations, including the application of self-composing operators with a specialized backbone architecture for the Helmholtz equation (detailed in Section 4) and an analysis of the proposed Train-and-Unroll strategy (introduced in Section 3), are presented in Section 5.

3. Dynamic depth training algorithm. In this section, we propose a novel training strategy for deep self-composed neural operators, termed the **Train-and-Unroll** approach. Instead of training a deep model with fixed depth directly, **Train-and-Unroll** incrementally increases the number of self-compositions during training, starting from a shallow architecture.

Motivation. Training deep neural operators $\mathcal{O}^{(\ell)} = \mathcal{P} \circ (\mathcal{G}_\theta \circ)^\ell \circ \mathcal{L}$ presents significant challenges where θ denotes all parameters in $\mathcal{G}(\cdot)$. Determining the optimal depth n a priori is difficult, and training very deep models directly can be computationally prohibitive. Verifying model selection and adjustments, particularly on large datasets, requires substantial computational resources. Furthermore, researchers often need to carefully balance model complexity (for computational efficiency) against predictive accuracy, sometimes prioritizing efficiency once minimum accuracy requirements are satisfied.

Our **Train-and-Unroll** strategy addresses these issues by incrementally increasing the depth ℓ during a single training process. We start by training a shallow model (e.g., $\ell = 1$). Then, we increase the depth (e.g., to $\ell = 2$) and continue training, using the previously learned weights of the shared operator \mathcal{G}_θ as an initialization. This leverages the model’s inherent structure for efficient training and allows for adaptive depth selection based on observed performance and computational budget. This approach is motivated by the observation that a deeper model $\mathcal{O}^{(d)}$ can often be effectively trained using weights from a converged shallower model $\mathcal{O}^{(s)}$ (where $s < d$). Such training may require only minimal fine-tuning.

Train-and-Unroll Strategy. Training deep neural operators, especially those with self-composing structures like $\mathcal{O}^{(\ell)} = \mathcal{P} \circ (\mathcal{G}_\theta \circ)^\ell \circ \mathcal{L}$, presents significant challenges. Determining the optimal composition depth ℓ a priori is difficult, and training very deep models directly can be computationally expensive and prone to optimization issues. To address these challenges, we propose an efficient training strategy called **Train-and-Unroll (T&U)**.

This strategy adaptively increases the composition depth ℓ of the *shared* backbone operator \mathcal{G}_θ during training. Specifically, it uses the weights learned for the operator \mathcal{G}_θ at depth $\ell - 1$ as a warm start for training the model at depth ℓ . At each depth ℓ , the parameters θ of the shared operator \mathcal{G}_θ are optimized by minimizing the mean

squared error loss:

$$\begin{aligned}
 \mathcal{L}(\theta; \ell) &= \frac{1}{N} \sum_{j=1}^N \left\| \mathcal{O}^{(\ell)}(\mathbf{u}_j) - \mathbf{v}_j \right\|^2 \\
 (3.1) \quad &= \frac{1}{N} \sum_{j=1}^N \left\| \mathcal{P} \circ (\mathcal{G}_\theta \circ)^\ell \circ \mathcal{L}(\mathbf{u}_j) - \mathbf{v}_j \right\|^2,
 \end{aligned}$$

where $(\mathbf{u}_j, \mathbf{v}_j)$ are input-output pairs from the training data, N is the number of training samples, and $\mathcal{O}^{(\ell)}(\mathbf{u}_j)$ represents the model's prediction for input \mathbf{u}_j using depth ℓ . This incremental approach leverages previously learned parameters, potentially leading to more efficient and stable training compared to training a fixed, deep model from scratch. The detailed algorithm is presented below.

Algorithm 3.1 Train-and-Unroll Algorithm

- 1: **Initialization:** Initialize \mathcal{G}_θ , \mathcal{P} , \mathcal{L} . Set initial model $\mathcal{O}^{(1)} := \mathcal{P} \circ (\mathcal{G}_\theta \circ)^1 \circ \mathcal{L}$.
 - 2: **Step 1:** Train $\mathcal{O}^{(1)}$ by minimizing $\mathcal{L}(\theta; 1)$ until convergence, yielding $\theta^{(1)}$.
 - 3: **Step 2:** Incrementally increase depth:
 - 4: **for** $\ell = 2$ to n **do**
 - 5: Initialize $\mathcal{O}^{(\ell)} := \mathcal{P} \circ (\mathcal{G}_{\theta^{(\ell-1)}} \circ)^\ell \circ \mathcal{L}$ using parameters $\theta^{(\ell-1)}$.
 - 6: Train $\mathcal{O}^{(\ell)}$ by minimizing $\mathcal{L}(\theta; \ell)$ until convergence, obtaining $\theta^{(\ell)}$.
 - 7: **end for**
 - 8: **Output:** A series of trained models $\mathcal{O}^{(1)}, \dots, \mathcal{O}^{(n)}$ with parameters $\theta^{(1)}, \dots, \theta^{(n)}$.
-

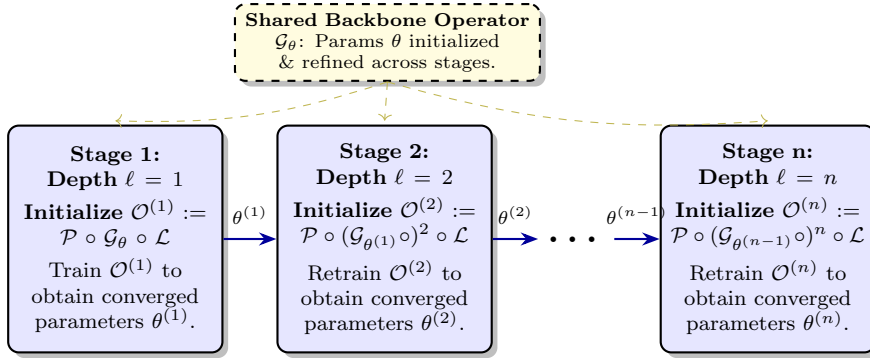


FIG. 1. Illustration of the Train-and-Unroll (T&U) strategy. The process starts with training a shallow model (Stage 1, depth $\ell = 1$). Converged parameters $\theta^{(1)}$ of the shared backbone \mathcal{G}_θ are then used to initialize \mathcal{G}_θ for a deeper model (Stage 2, depth $\ell = 2$), which is then trained. This incremental process of parameter transfer and retraining continues up to the desired depth n .

Novelty and Practical Advantages. The novelty of T&U lies in its adaptive, incremental training process specifically for the shared-parameter, variable-depth structure $\mathcal{P} \circ (\mathcal{G}_\theta \circ)^n \circ \mathcal{L}$. This yields significant practical benefits:

- **Computational and Memory Efficiency:** Training starts with shallower, less expensive models. The weight transfer provides a warm start, potentially accelerating convergence for deeper models compared to training from scratch, leading to reduced overall training time and memory usage (activations).

- **Adaptive Depth Selection:** T&U naturally outputs models $\mathcal{O}^{(1)}, \dots, \mathcal{O}^{(n)}$. Practitioners can monitor performance and stop at an intermediate depth $\ell < n$ if satisfactory accuracy is achieved, avoiding unnecessary computation for potentially excessive depths.
- **Improved Optimization:** The gradual increase in depth acts as a curriculum, potentially stabilizing training and guiding the optimizer towards better solutions compared to tackling the full depth immediately.
- **Flexibility and Scalability:** An existing model $\mathcal{O}^{(\ell)}$ can be readily extended and fine-tuned to a deeper $\mathcal{O}^{(\ell+k)}$ if requirements change, without restarting training.

Convergence Behavior. The empirical convergence behavior of the Train-and-Unroll (T&U) strategy is illustrated in Figure 2. Figure 2(a) compares the training loss dynamics between the T&U method as in Algorithm 3 (red curve) and conventional direct training (blue curve). The T&U approach begins with a shallow model (e.g., $\ell = 3$) and progressively increases depth (e.g., to $\ell = 4$, then $\ell = 5$). At each depth transition, the training loss initially increases because the model depth increments by one while the weights remain unchanged. However, the loss rapidly decreases to levels even lower than the final training error of the previous stage within just a few optimization steps, as demonstrated by the steep, almost vertical descent lines in the plot. We hypothesize that at each depth increment, the weights from the converged shallower model provide an effective warm start due to the specific self-composing architecture, enabling the deeper model to quickly achieve its enhanced expressivity through minimal fine-tuning. Although T&U may initially converge more slowly due to its shallow initialization, it efficiently reuses learned representations to achieve a final training loss comparable to direct training at the target depth (e.g., $\ell = 5$) from scratch, demonstrating both effectiveness and computational efficiency. Figure 2(b) then illustrates the training error reduction as model depth ℓ increases, using the final training error achieved at each T&U stage. This observation aligns with theoretical expectations (cf. Theorem 2.3) and reflects the iterative error-decaying property of the self-composing architecture.

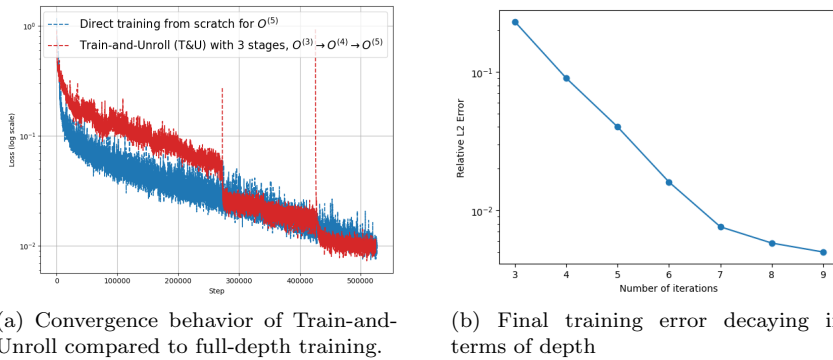


FIG. 2. Convergence behavior of Train-and-Unroll compared to full-depth training. The error convergence plot shows the error decay with increasing depth ℓ .

4. An application to ultrasound computed tomography with specific backbone architecture. In this section, we propose a specific architecture for the backbone operator \mathcal{G}_θ within the self-composing neural operator framework $\mathcal{O}(\mathbf{v}) =$

$\mathcal{P} \circ (\mathcal{G}_\theta \circ)^n \circ \mathcal{L}(\mathbf{v})$, tailored for solving the Helmholtz equation arising in ultrasound computed tomography (USCT).

4.1. Operator learning task for Helmholtz equation. In many physical problems, the input data consists of multiple fields, such as the wavenumber field $k(x)$ and the source term $f(x)$ in the Helmholtz equation. The neural operator should be able to learn the mapping from these multiple fields to the output field $u(x)$, which satisfies the governing equation.

Let $\Omega \subset \mathbb{R}^d$ ($d = 2, 3$) be a bounded Lipschitz domain with boundary Γ and outward normal n . Given a variable wavenumber field $k \in L^\infty(\Omega)$ with $0 < k_{\min} \leq k(x) \leq k_{\max} < \infty$, and a boundary wavenumber $k|_\Gamma > 0$. Given a source $f \in L^2(\Omega)$, find $u \in H^1(\Omega)$ such that

$$(4.1) \quad \begin{cases} -\Delta u - k(x)^2 u = f & \text{in } \Omega, \\ \partial_n u - i k|_\Gamma u = 0 & \text{on } \Gamma. \end{cases}$$

For our numerical experiments on this task, we utilize the **OpenBreastUS** dataset, a comprehensive benchmark for wave imaging in breast ultrasound computed tomography recently introduced by Zeng et al. [51]. This dataset presents significant challenges due to the highly heterogeneous and multiscale nature of the wavenumber fields, which model different breast tissues. Accurately resolving the complex wave scattering and diffraction phenomena in such media is a difficult task for neural operators, making it an excellent testbed for evaluating model performance [2].

Following the self-composition paradigm motivated by iterative solvers, we aim to learn a backbone operator \mathcal{G}_θ such that repeated application approximates the solution. Let $\mathbf{u}, \mathbf{k}, \mathbf{f}$ be the discretized fields. We learn \mathcal{G}_θ such that the final solution \mathbf{u} is approximated by \mathbf{u}^n obtained via the iteration:

$$(4.2) \quad \mathbf{u}^i = \mathcal{G}_\theta(\mathbf{u}^{i-1}, \mathbf{k}, \mathbf{f}), \quad i = 1, \dots, n$$

with an initial state \mathbf{u}^0 (e.g., $\mathbf{u}^0 = 0$). The overall operator mapping (\mathbf{k}, \mathbf{f}) to \mathbf{u}^n fits the form $\mathcal{P} \circ (\mathcal{G}_\theta \circ)^n \circ \mathcal{L}$, where \mathcal{L} incorporates \mathbf{k}, \mathbf{f} and sets \mathbf{u}^0 , and \mathcal{P} simply extracts the final state \mathbf{u}^n .

4.2. Multigrid-inspired backbone architecture. For the Helmholtz problem, the backbone operator \mathcal{G}_θ is inspired by multigrid methods. The operator \mathcal{G}_θ updates a solution estimate \mathbf{u}^{i-1} to \mathbf{u}^i using the wavenumber field \mathbf{k} and source term \mathbf{f} , employing a residual update. Its core is a multigrid V-cycle. This V-cycle utilizes learnable components. The inter-grid transfer operators are learnable: restriction \mathcal{R}_{2h}^h is implemented as a 2D convolution with stride 2 (e.g., kernel size 3x3, padding 1, preserving channel dimensions), and prolongation \mathcal{P}_h^{2h} is implemented as a 2D transposed convolution with stride 2 (e.g., kernel size 3x3, padding 1, also preserving channel dimensions). Activation functions (e.g., GELU) are used throughout the network.

Central to the V-cycle are the learnable PDE operator \mathcal{A}_h and the learnable smoother \mathcal{S}_h , applied at each grid level h . Both \mathcal{A}_h and \mathcal{S}_h are realized using distinct instantiations of the Adaptive Convolution Mechanism (detailed in Section 4.3). Specifically, $\mathcal{A}_h(\mathbf{k}_h, \mathbf{u}_h)$ uses one set of convolution parameters (e.g., $\text{Filters}_A, \text{MLP}_A$) to approximate the PDE operator, and $\mathcal{S}_h(\mathbf{k}_h, \mathbf{r}_h)$ uses another set (e.g., $\text{Filters}_S, \text{MLP}_S$) for smoothing. The smoother \mathcal{S}_h is designed to be linear concerning the residual \mathbf{r}_h it processes, but non-linear concerning \mathbf{k}_h , effectively dampening errors

across various frequencies. Similarly, \mathcal{A}_h is non-linear with respect to \mathbf{k}_h while aiming for linearity with respect to \mathbf{u}_h to correctly model the Helmholtz operator.

A single V-cycle operation, processing an input solution \mathbf{u}_h on a grid h , involves the following steps:

- **Pre-smoothing:** First, calculate the residual based on the current solution \mathbf{u}_h :

$$(4.3) \quad \mathbf{r}_h = \mathbf{f}_h - \mathcal{A}_h(\mathbf{k}_h, \mathbf{u}_h),$$

where \mathcal{A}_h is the learnable PDE operator (an instance of Adaptive Convolution) that incorporates the wavenumber field \mathbf{k}_h and the current solution \mathbf{u}_h to mimic the Helmholtz equation $-\Delta \mathbf{u}_h - k_h^2 \mathbf{u}_h = \mathbf{f}_h$ on the grid h . Then, apply the smoother \mathcal{S}_h (another instance of Adaptive Convolution) using this residual to update the solution, reducing high-frequency error:

$$(4.4) \quad \mathbf{u}_h \leftarrow \mathbf{u}_h + \mathcal{S}_h(\mathbf{k}_h, \mathbf{r}_h).$$

Let this updated solution be \mathbf{u}_h^{sm} .

- **Residual Restriction:** The residual computed by equation 4.3 (i.e., \mathbf{r}_h , before the pre-smoothing update was applied to \mathbf{u}_h) is restricted to a coarser grid $2h$ using the learnable restriction operator \mathcal{R}_{2h}^h (strided convolution):

$$(4.5) \quad \mathbf{r}_{2h} = \mathcal{R}_{2h}^h \mathbf{r}_h.$$

The \mathbf{k}_h is also restricted to the coarse grid, typically using an operation like average pooling or strided convolution, yielding \mathbf{k}_{2h} .

- **Coarse-Grid Problem:** Recursively apply the V-cycle for the coarse-grid problem, aiming to solve for an error correction \mathbf{e}_{2h} such that $\mathcal{A}_{2h}(\mathbf{k}_{2h}, \mathbf{e}_{2h}) \approx \mathbf{r}_{2h}$, yielding an approximate error correction \mathbf{e}_{2h}^* . At the coarsest grid level, the smoother \mathcal{S}_H (where H is the coarsest grid size) is typically applied multiple times (e.g., 2-4 iterations).
- **Prolongation and Correction:** Interpolate the computed error correction \mathbf{e}_{2h}^* from the coarse grid back to the fine grid using the learnable prolongation operator \mathcal{P}_h^{2h} (transposed convolution): $\mathbf{e}_h = \mathcal{P}_h^{2h} \mathbf{e}_{2h}^*$. Update the fine-grid solution by adding this correction to the pre-smoothed solution: $\mathbf{u}_h \leftarrow \mathbf{u}_h^{sm} + \mathbf{e}_h$. Let this be \mathbf{u}_h^{corr} .
- **Post-smoothing:** Apply the smoother \mathcal{S}_h again on the fine grid to further refine the solution \mathbf{u}_h^{corr} . This involves computing a new residual $\mathbf{r}_h^{new} = \mathbf{f}_h - \mathcal{A}_h(\mathbf{k}_h, \mathbf{u}_h^{corr})$ and then updating $\mathbf{u}_h \leftarrow \mathbf{u}_h^{corr} + \mathcal{S}_h(\mathbf{k}_h, \mathbf{r}_h^{new})$.

This recursive process allows \mathcal{G}_θ to efficiently address multi-frequency errors. The global dependence of the wave solution on $k(x)$ is learned through the learnable components: the PDE operator \mathcal{A}_h , the smoother \mathcal{S}_h , the restriction operator \mathcal{R}_{2h}^h , and the prolongation operator \mathcal{P}_h^{2h} at each level. The adaptive components \mathcal{A}_h and \mathcal{S}_h are particularly key, as they adapt to local wave characteristics influenced by $k(x)$. We next detail the Adaptive Convolution Mechanism that forms the basis for \mathcal{S}_h and \mathcal{A}_h .

4.3. Adaptive convolution mechanism (AdaConv). As mentioned, this Adaptive Convolution Mechanism is the core building block for both the learnable PDE operator \mathcal{A}_h and the learnable smoother \mathcal{S}_h within the V-cycle, each typically with its own set of learnable parameters (Filters, MLP). To effectively incorporate

the spatially varying wavenumber field $k(x)$ (discretized as \mathbf{k}) into the learned operator, we introduce an Adaptive Convolution Mechanism. This mechanism enables the network to modulate its processing of a primary field (e.g., wave field estimate \mathbf{u} or residual \mathbf{r}) based on the local values of \mathbf{k} .

Let \mathbf{x} represent the primary input field (e.g., \mathbf{u} or \mathbf{r}) and \mathbf{k} represent the wavenumber field. The Adaptive Convolution is defined as:

$$(4.6) \quad \text{AdaConv}(\mathbf{k}, \mathbf{x}; \text{Filter}_k, \text{Filter}_x, \text{MLP}) = (\text{MLP}(\text{Filter}_k * \mathbf{k})) \odot (\text{Filter}_x * \mathbf{x})$$

Here, $*$ denotes standard convolution, and \odot represents element-wise multiplication. Filter_x and Filter_k are learnable convolutional filters (e.g., 3x3 kernels, mapping C channels to C channels), while the MLP is a small multi-layer perceptron (e.g., 2 layers, $C \rightarrow C$ channels, with GELU activation) applied point-wise to the feature maps derived from \mathbf{k} .

Mechanism and relation to other methods: As defined in Equation equation 4.6, the Adaptive Convolution Mechanism processes \mathbf{k} and \mathbf{x} through their respective convolutional layers ($\text{Filter}_k, \text{Filter}_x$). The output derived from \mathbf{k} after being processed by Filter_k and the MLP, i.e., $\text{MLP}(\text{Filter}_k * \mathbf{k})$, serves as spatially varying multiplicative weights. These weights modulate the features obtained from processing \mathbf{x} with Filter_x . This allows the network’s response to adapt based on the local wavenumber field, effectively scaling the features of the primary field \mathbf{x} according to the wavenumber field \mathbf{k} . When \mathbf{x} is the residual \mathbf{r}_h (as in the smoother \mathcal{S}_h), this mechanism modulates the residual features. At coarser grid levels, this mechanism allows the network to learn the scattering effects of the wavenumber field \mathbf{k}_H on the wave field or error correction, which is crucial for accurately modeling wave propagation in heterogeneous media.

It is important to distinguish this mechanism from Dynamic or Conditional Convolution methods [27, 48, 7]. These latter approaches dynamically generate convolutional filter weights based on the input, directly adapting the convolution operation. In contrast, our Adaptive Convolution Mechanism employs fixed, shared convolutional filters (Filter_x and Filter_k). Adaptation is achieved not by altering these kernels, but by modulating the feature maps resulting from $\text{Filter}_x * \mathbf{x}$ through element-wise multiplication with adaptive weights derived from \mathbf{k} (specifically, $\text{MLP}(\text{Filter}_k * \mathbf{k})$). This design is motivated by the physical intuition that the wavenumber field $k(x)$ locally influences wave propagation characteristics, which can be modeled by modulating the wave field using $k(x)$ field [39].

5. Numerical experiments. We evaluate our proposed self-composing neural operator, termed MgNO-self, on a challenging ultrasound computed tomography (USCT) task. This task involves solving the Helmholtz equation (as described in Section 4.1 by Equation equation 4.1), where the model maps a given wave number field $k(x)$ and a source term $f(x)$ to the corresponding wave field solution $u(x)$. The MgNO-self utilizes the multigrid-inspired backbone architecture detailed in Section 4.2.

From the results in Table 2, it is evident that the MgNO-self model consistently and significantly outperforms all other baseline models across all tested frequencies and both error metrics.

Qualitative results are presented in Figure 4, which illustrates the capability of the MgNO-self model to accurately predict wave field solutions for different input configurations. Each row in the figure typically displays the input sound speed field

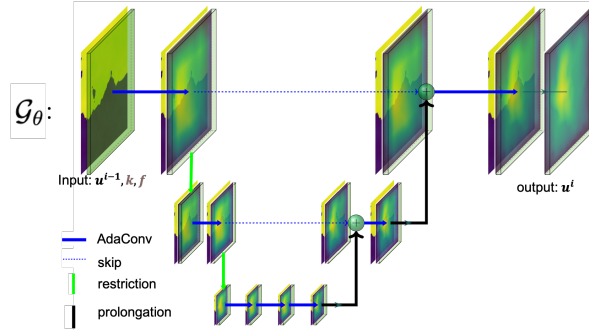


FIG. 3. The diagram on the right illustrates the general architecture of the self-composing neural operator, expressed as $\mathcal{P} \circ (\mathcal{G}_\theta \circ)^n \circ \mathcal{L}$. On the left is the specific Multigrid-inspired backbone \mathcal{G}_θ designed for the Helmholtz application. A key feature is the Adaptive Convolution Mechanism (AdaConv), which distinguishes it from prior works such as [22, 21].

Frequency (kHz)	Metric	Models				
		UNet	FNO	AFNO	BFNO	MgNO-self
300	RRMSE	0.1236	0.0269	0.0165	0.0113	0.0028
	Max Error	0.2551	0.0617	0.0293	0.0519	0.0092
400	RRMSE	0.1503	0.0426	0.0242	0.0148	0.0036
	Max Error	0.3017	0.1172	0.0464	0.0840	0.0178
500	RRMSE	0.1798	0.0490	0.0276	0.0209	0.0049
	Max Error	0.3571	0.1432	0.0639	0.0838	0.0262

TABLE 2

Quantitative evaluation of forward simulation baselines on ultrasound computed tomography (USCT) task. Performance was evaluated on the test set using Relative Root Mean Square Error (RRMSE) and Maximum Error (Max Error). Our MgNO-self model is compared against several established baseline models: UNet, FNO, AFNO[15], and BFNO [53]. The evaluation is performed on the forward simulation task across three different wave frequencies (300 kHz, 400 kHz, and 500 kHz). This USCT task is also comprehensively benched in [51], where MgNO-self mode is named after MgNO.

(related to the wave number k), the groundtruth wave field solution \mathbf{u} for a specific source term \mathbf{f} , and the corresponding wave field solution predicted by MgNO-self. The visualizations demonstrate that the model effectively captures complex wave phenomena, including scattering effects due to inhomogeneous sound speed distributions, and accurately reproduces the wave field structure.

6. Conclusions and future work. In this work, we introduced self-composing neural operators, a novel framework that builds deep models by repeatedly applying a single, parameter-efficient backbone block, inspired by classical iterative solvers. To enable effective learning, we proposed the Train-and-Unroll (T&U) strategy, an adaptive curriculum that incrementally increases model depth during training. Our approach is validated by both theory and strong empirical results. We proved that self-composing operators are universal approximators and that deeper compositions reduce error. In practice, our models achieve significant parameter efficiency on Darcy flow benchmarks and state-of-the-art performance on a challenging Helmholtz equation task, demonstrating their power and scalability. While our theoretical error-reduction rate of $O(1/\log(n))$ guarantees convergence, the much faster decay observed empirically presents a compelling avenue for future investigation. The flexibility of the self-composition paradigm opens the door to using other backbones, like transformers, and tackling a wider range of scientific problems. We believe this work offers

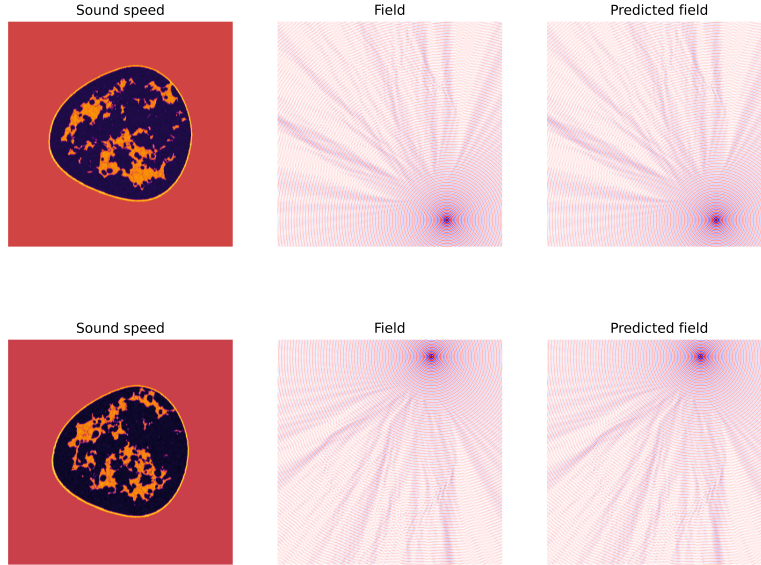


FIG. 4. Wave field solutions for different configurations. The left column shows the sound speed field vk , the middle column shows the groundtruth wavefield \mathbf{u} with specific source term \mathbf{f} , and the right column shows the predicted wave field solution. The neural operator can take different sound speed fields and the location of point sources as the input and output the wave field solutions, which have obvious scattering because of the inhomogeneous sound speed.

a promising path toward developing more efficient, scalable, and physically-grounded neural operators.

REFERENCES

- [1] S. BAI, J. Z. KOLTER, AND V. KOLTUN, *Deep equilibrium models*, Advances in neural information processing systems, 32 (2019).
- [2] J. A. L. BENITEZ, T. FURUYA, F. FAUCHER, A. KRATSIOS, X. TRICOCHÉ, AND M. V. DE HOOP, *Out-of-distributional risk bounds for neural operators with applications to the helmholtz equation*, Journal of Computational Physics, 513 (2024), p. 113168.
- [3] S. CAO, *Choose a transformer: Fourier or galerkin*, Advances in Neural Information Processing Systems, 34 (2021).
- [4] G. CHEN, X. LIU, Q. MENG, L. CHEN, C. LIU, AND Y. LI, *Learning neural operators on riemannian manifolds*, arXiv preprint arXiv:2302.08166, (2023).
- [5] J.-S. CHEN, C. PAN, C.-T. WU, AND W. K. LIU, *Reproducing kernel particle methods for large deformation analysis of non-linear structures*, Computer Methods in Applied Mechanics and Engineering, 139 (1996), pp. 195–227.
- [6] R. T. CHEN, Y. RUBANOVA, J. BETTENCOURT, AND D. K. DUVENAUD, *Neural ordinary differential equations*, Advances in neural information processing systems, 31 (2018).
- [7] Y. CHEN, X. DAI, M. LIU, D. CHEN, L. YUAN, AND Z. LIU, *Dynamic convolution: Attention over convolution kernels*, in Proceedings of the IEEE/CVF conference on computer vision and pattern recognition, 2020, pp. 11030–11039.
- [8] Y. CHEN, B. DONG, AND J. XU, *Meta-mgnet: Meta multigrid networks for solving parameterized partial differential equations*, Journal of computational physics, 455 (2022), p. 110996.
- [9] J. T. CONNOR, R. D. MARTIN, AND L. E. ATLAS, *Recurrent neural networks and robust time series prediction*, IEEE Transactions on Neural Networks, 5 (1994), pp. 240–254.
- [10] X. DING, X. ZHANG, J. HAN, AND G. DING, *Scaling up your kernels to 31x31: Revisiting large*

- kernel design in cnns*, in Proceedings of the IEEE/CVF conference on computer vision and pattern recognition, 2022, pp. 11963–11975.
- [11] W. E, *A Proposal on Machine Learning via Dynamical Systems*, Communications in Mathematics and Statistics, 5 (2017), pp. 1–11.
 - [12] S. W. FUNG, H. HEATON, Q. LI, D. MCKENZIE, S. OSHER, AND W. YIN, *Jfb: Jacobian-free backpropagation for implicit networks*, in Proceedings of the AAAI Conference on Artificial Intelligence, vol. 36, 2022, pp. 6648–6656.
 - [13] Z. GENG, X.-Y. ZHANG, S. BAI, Y. WANG, AND Z. LIN, *On training implicit models*, Advances in Neural Information Processing Systems, 34 (2021), pp. 24247–24260.
 - [14] K. GREGOR AND Y. LECUN, *Learning fast approximations of sparse coding*, in Proceedings of the 27th international conference on international conference on machine learning, 2010, pp. 399–406.
 - [15] J. GUIBAS, M. MARDANI, Z. LI, A. TAO, A. ANANDKUMAR, AND B. CATANZARO, *Adaptive fourier neural operators: Efficient token mixers for transformers*, arXiv preprint arXiv:2111.13587, (2021).
 - [16] G. GUPTA, X. XIAO, AND P. BOGDAN, *Multiwavelet-based operator learning for differential equations*, Advances in Neural Information Processing Systems, 34 (2021), pp. 24048–24062.
 - [17] E. HABER, L. RUTHOTTO, E. HOLTHAM, AND S.-H. JUN, *Learning across scales—multiscale methods for convolution neural networks*, in Proceedings of the AAAI conference on artificial intelligence, vol. 32, 2018.
 - [18] W. HACKBUSCH, *Multi-grid methods and applications*, vol. 4, Springer Science & Business Media, 2013.
 - [19] W. HAO, X. LIU, AND Y. YANG, *Newton informed neural operator for solving nonlinear partial differential equations*, in Advances in Neural Information Processing Systems, vol. 37, 2024.
 - [20] Z. HAO, Z. WANG, H. SU, C. YING, Y. DONG, S. LIU, Z. CHENG, J. SONG, AND J. ZHU, *Gnot: A general neural operator transformer for operator learning*, in International Conference on Machine Learning, PMLR, 2023, pp. 12556–12569.
 - [21] J. HE, X. LIU, AND J. XU, *Mgno: Efficient parameterization of linear operators via multigrid*, in International Conference on Learning Representations, 2024.
 - [22] J. HE AND J. XU, *Mgnet: A unified framework of multigrid and convolutional neural network*, Science China Mathematics, (2019), pp. 1–24.
 - [23] J. HE, J. XU, L. ZHANG, AND J. ZHU, *An interpretive constrained linear model for resnet and mgnet*, Neural Networks, 162 (2023), pp. 384–392.
 - [24] K. HE, X. ZHANG, S. REN, AND J. SUN, *Deep residual learning for image recognition*, in Proceedings of the IEEE Conference on Computer Vision and Pattern Recognition, 2016, pp. 770–778.
 - [25] K. HE, X. ZHANG, S. REN, AND J. SUN, *Identity mappings in deep residual networks*, in European Conference on Computer Vision, Springer, 2016, pp. 630–645.
 - [26] J. HU AND P. JIN, *A hybrid iterative method based on mionet for pdes: Theory and numerical examples*, Mathematics of Computation, (2025).
 - [27] X. JIA, B. DE BRABANDERE, T. TUYTELAARS, AND L. VAN GOOL, *Dynamic filter networks*, in Advances in neural information processing systems, 2016, pp. 667–675.
 - [28] P. JIN, S. MENG, AND L. LU, *Mionet: Learning multiple-input operators via tensor product*, SIAM Journal on Scientific Computing, 44 (2022), pp. A3490–A3514.
 - [29] N. KOVACHKI, Z. LI, B. LIU, K. AZIZZADENESHELI, K. BHATTACHARYA, A. STUART, AND A. ANANDKUMAR, *Neural operator: Learning maps between function spaces*, arXiv preprint arXiv:2108.08481, (2021).
 - [30] N. KOVACHKI, Z. LI, B. LIU, K. AZIZZADENESHELI, K. BHATTACHARYA, A. STUART, AND A. ANANDKUMAR, *Neural operator: Learning maps between function spaces with applications to pdes*, Journal of Machine Learning Research, 24 (2023), pp. 1–97.
 - [31] S. LANTHALER, Z. LI, AND A. M. STUART, *The nonlocal neural operator: Universal approximation*, arXiv preprint arXiv:2304.13221, (2023).
 - [32] Z. LI, D. Z. HUANG, B. LIU, AND A. ANANDKUMAR, *Fourier neural operator with learned deformations for pdes on general geometries*, arXiv preprint arXiv:2207.05209, (2022).
 - [33] Z. LI, N. B. KOVACHKI, K. AZIZZADENESHELI, K. BHATTACHARYA, A. STUART, AND A. ANANDKUMAR, *Fourier NeuralOperator for Parametric Partial Differential Equations*, in International Conference on Learning Representations, 2020.
 - [34] X. LIU, B. XU, S. CAO, AND L. ZHANG, *Mitigating spectral bias for the multiscale operator learning*, Journal of Computational Physics, 506 (2024), p. 112944.
 - [35] L. LU, P. JIN, G. PANG, Z. ZHANG, AND G. E. KARNIADAKIS, *Learning nonlinear operators via DeepONet based on the universal approximation theorem of operators*, Nature Machine

- Intelligence, 3 (2021), pp. 218–229.
- [36] Y. LU, A. ZHONG, Q. LI, AND B. DONG, *Beyond finite layer neural networks: Bridging deep architectures and numerical differential equations*, in International Conference on Machine Learning, PMLR, 2018, pp. 3276–3285.
 - [37] H. LUO, H. WU, H. ZHOU, L. XING, Y. DI, J. WANG, AND M. LONG, *Transolver++: An accurate neural solver for pdes on million-scale geometries*, arXiv preprint arXiv:2502.02414, (2025).
 - [38] T. MARWAH, A. POKLE, J. Z. KOLTER, Z. LIPTON, J. LU, AND A. RISTESKI, *Deep equilibrium based neural operators for steady-state pdes*, Advances in Neural Information Processing Systems, 36 (2023), pp. 15716–15737.
 - [39] G. OSNABRUGGE, S. LEEDUMRONGWATTHANAKUN, AND I. M. VELLEKOOP, *A convergent born series for solving the inhomogeneous helmholtz equation in arbitrarily large media*, Journal of computational physics, 322 (2016), pp. 113–124.
 - [40] J. PATHAK, S. SUBRAMANIAN, P. HARRINGTON, S. RAJA, A. CHATTOPADHYAY, M. MARDANI, T. KURTH, D. HALL, Z. LI, K. AZIZZADENESHELI, ET AL., *Fourcastnet: A global data-driven high-resolution weather model using adaptive fourier neural operators*, arXiv preprint arXiv:2202.11214, (2022).
 - [41] M. A. RAHMAN, Z. E. ROSS, AND K. AZIZZADENESHELI, *U-no: U-shaped neural operators*, arXiv e-prints, (2022), pp. arXiv–2204.
 - [42] B. RAONIC, R. MOLINARO, T. ROHNER, S. MISHRA, AND E. DE BEZENAC, *Convolutional neural operators*, in ICLR 2023 Workshop on Physics for Machine Learning, 2023.
 - [43] O. RONNEBERGER, P. FISCHER, AND T. BROX, *U-net: Convolutional networks for biomedical image segmentation*, in International Conference on Medical image computing and computer-assisted intervention, Springer, 2015, pp. 234–241.
 - [44] U. TROTTEMBERG, C. W. OOSTERLEE, AND A. SCHULLER, *Multigrid*, Elsevier, 2000.
 - [45] A. VASWANI, N. SHAZEER, N. PARMAR, J. USZKOREIT, L. JONES, A. N. GOMEZ, L. KAISER, AND I. POLOSUKHIN, *Attention is all you need*, Advances in neural information processing systems, 30 (2017).
 - [46] H. WU, T. HU, H. LUO, J. WANG, AND M. LONG, *Solving high-dimensional pdes with latent spectral models*, arXiv preprint arXiv:2301.12664, (2023).
 - [47] J. XU, *Theory of multilevel methods*, vol. 8924558, Cornell University, 1989.
 - [48] B. YANG, G. BENDER, Q. V. LE, AND J. NGIAM, *Condconv: Conditionally parameterized convolutions for efficient inference*, in Advances in neural information processing systems, 2019, pp. 1305–1316.
 - [49] H. YOU, Q. ZHANG, C. J. ROSS, C.-H. LEE, M.-C. HSU, AND Y. YU, *A physics-guided neural operator learning approach to model biological tissues from digital image correlation measurements*, Journal of Biomechanical Engineering, accepted for publication, (2022), p. arXiv preprint arXiv:2204.00205.
 - [50] C. ZENG, Y. ZHANG, J. ZHOU, Y. WANG, Z. WANG, Y. LIU, L. WU, AND D. Z. HUANG, *Point cloud neural operator for parametric pdes on complex and variable geometries*, arXiv preprint arXiv:2501.14475, (2025).
 - [51] Z. ZENG, Y. ZHENG, H. HU, Z. DONG, Y. ZHENG, X. LIU, J. WANG, Z. SHI, L. ZHANG, Y. LI, ET AL., *Openbreastus: Benchmarking neural operators for wave imaging using breast ultrasound computed tomography*, arXiv preprint arXiv:2507.15035, (2025).
 - [52] S. ZHANG, J. LU, AND H. ZHAO, *On enhancing expressive power via compositions of single fixed-size relu network*, in International Conference on Machine Learning, PMLR, 2023, pp. 41452–41487.
 - [53] Q. ZHAO, Y. MA, P. BOUFONOS, S. NABI, AND H. MANSOUR, *Deep born operator learning for reflection tomographic imaging*, in ICASSP 2023-2023 IEEE International Conference on Acoustics, Speech and Signal Processing (ICASSP), IEEE, 2023, pp. 1–5.
 - [54] J. ZHU, J. HE, AND Q. HUANG, *An enhanced v-cycle mgnet model for operator learning in numerical partial differential equations*, Computational Geosciences, (2023), pp. 1–12.
 - [55] J. ZHU, J. HE, L. ZHANG, AND J. XU, *Fv-mgnet: Fully connected v-cycle mgnet for interpretable time series forecasting*, Journal of Computational Science, 69 (2023), p. 102005.